31st Annual International Conference of the IEEE EMBS
Minneapolis, Minnesota, USA, September 2-6, 2009

# Full Dimensional Computer Simulations to Study Pulsatile Blood Flow in Vessels, Aortic Arch and Bifurcated Veins: Investigation of Blood Viscosity and Turbulent Effects

Renat A. Sultanov and Dennis Guster

*Abstract*— **We report computational results of blood flow through a model of the human aortic arch and a vessel of actual diameter and length. A realistic pulsatile flow is used in all simulations. Calculations for bifurcation type vessels are also carried out and presented. Different mathematical methods for numerical solution of the fluid dynamics equations have been considered. The non-Newtonian behaviour of the human blood is investigated together with turbulence effects. A detailed time-dependent mathematical convergence test has been carried out. The results of computer simulations of the blood flow in vessels of three different geometries are presented: for pressure, strain rate and velocity component distributions we found significant disagreements between our results obtained with realistic non-Newtonian treatment of human blood and the widely used method in the literature: a simple Newtonian approximation. A significant increase of the strain rate and, as a result, the wall shear stress distribution, is found in the region of the aortic arch. Turbulent effects are found to be important, particularly in the case of bifurcation vessels.**

## I. INTRODUCTION

Human blood is a liquid with density and viscosity that is altered by the body, based on physiologic needs and disease states. The movement of the blood, that is hemodynamics, inside vessels and arteries can be described by fundamental laws of physics, i.e. equations of fluid dynamics. The scientific literature now contains many citations where researchers have used computer simulation of blood flow in various size vessels and arteries with different spatial geometries where experimental investigations of vascular dynamics and flow are complicated or simply impossible to carry out (due to small sizes of vessels) in living systems. Therefore, theoretical mathematical models and computer simulations are very useful for studying blood flow to understand situations related to health and disease [1].

Cardiovascular diseases, such as ischemic heart disease, myocardial infarction, and stroke are leading causes of death in Western countries. All of these vascular diseases share a common element: atherosclerosis. They also share a common final event: the failure or destruction of the vascular wall structure [2].

Atherosclerosis reduces arterial lumen size through plaque formation and arterial wall thickening and it occurs at specific arterial sites. This phenomenon is related to hemodynamics and to wall shear stress (WSS) distribution. From the physical point of view WSS is the tangential drag force produced by moving blood, and it is a mathematical function of the velocity gradient of blood near the endothelial surface [3]. Arterial wall remodeling is regulated by WSS. For example, in response to high shear stress arteries enlarge. Currently researchers in the field of biomechanics and biomedicine conduct laboratory investigations of human blood flow in different shape and size tubes, which are designed to be approximate models of human vessels and arteries, see for example [1]. Some researchers also carry out intensive computer simulations of these bio-mechanical systems, see for example [4], [5], [6].

Also, in some special laboratory works specific stents are implanted in such artifical vessels (tubes). Stent implantation has been used to open diseased coronary blood vessels, allowing improved perfusion of the cardiac muscle. Used in combination with drug therapy, vascular repair and dilation techniques (angioplasty) the use of metallic stents has created a multibillion dollar industry. Stents are commonly used in many different blood vessels, but the primary site of deployment is in diseased coronary arteries.

Stents represent a very special case in the modeling problems mentioned above [7]. Taking into account that stents have a very small size and rather complicated structure and shape, this situation makes it difficult to obtain precise measurements. Therefore high quality and precise computer simulation of blood flow through vessels with implanted stents would be most useful [7], [8].

Nevertheless, there are still many difficulties in obtaining precise realistic geometries for the required vessels. Human arteries, especially the aorta, have complicated spatial-geometric and characteristic configurations. For example, the aortic arch centerline does not lie on a plane and there are major branches at the top of the arch feeding the carotid arterial circulation. One of the main problems in the field of bio-medical blood flow simulation is to obtain precise geometrical-mathematical representations of different vessels. This information in turn needs to be included in the simulation programs.

However, in our opinion, as a first step of these investigations it would be useful to apply simpler 3D-geometry forms and models, but to take into account the precise physical effects of blood movement such as the non-Newtonian characteristics of human blood, realistic pulsatile flow, and

Renat A. Sultanov is with Business Computing Research Laboratory, St. Cloud State University, St. Cloud, MN 56301, USA rasultanov@stcloudstate.edu

Dennis Guster is with Business Computer Information Systems, St. Cloud State University, St. Cloud, MN 56301, USA dcguster@stcloudstate.edu

 

possible turbulent effects. Because of pulsatility turbulence may be significant in the final results of this study.

In the current work we carried out real-time full-dimensional computer simulations of realistic pulsatile human blood flow in actual size vessels, vessels with a bifurcation, and in a model of the aortic arch. We take into account different physical effects, such as turbulence and the non-Newtonian nature of human blood. The next section presents the mathematical methodology and the physical model used in this work. The general purpose commercial computational fluid dynamics program FLOW3D is used for its basic functionality, but we supplemented its capability by adding routines to obtain the results presented herein. Sec. II presents results for three vessels of different geometries. The CGS unit system is used in all simulations, as well as for presentation of the results.

## II. MATHEMATICAL METHODOLOGY AND PHYSICAL MODELS

As we mentioned above, we undertook pulsatile human blood flow simulation experiments using different size and shape human vessels/arteries. For each spatial configuration one needs to devise a specific approach to obtain the numerical solution to the complicated second order partial differential equations of fluid dynamics (FD). For example, for simple cylindrical vessels we used the cylindrical coordinate system: $\vec{r} = (r, \theta, \phi)$. However, for the aortic arch or bifurcated vessels, where there is no cylindrical symmetry, we applied the Cartesian coordinate system: $\vec{r} = (x, y, z)$. For the aortic arch and bifurcated vessels we used up to five blocks of matched Cartesian coordinate subsystems.

Below we present the FD equations in a general form, because for each of the special cases considered in this work and the chosen coordinate system, the partial differential equations of fluid dynamics may look different. However we understand, that the general differential operator form of the equations is always unique.

### A. Equations

The equations of motion for the fluid velocity components $(u, v, w)$ in the 3-coordinate system are the Navier-Stokes equations with specific additional terms included in the FLOW3D program:

$$\frac{\partial u}{\partial t} + \frac{1}{V_F}(uA_x\frac{\partial u}{\partial x} + vA_yR\frac{\partial u}{\partial y} + wA_z\frac{\partial u}{\partial z}) - \xi\frac{A_yv^2}{xV_f} = -\frac{1}{\rho}\frac{\partial p}{\partial x} + G_x + f_x - b_x - \frac{R_{sor}}{\rho V_f}(u - u_w - \delta\cdot u_s) \quad (1)$$

$$\frac{\partial v}{\partial t} + \frac{1}{V_F}(uA_x\frac{\partial v}{\partial x} + vA_yR\frac{\partial v}{\partial y} + wA_z\frac{\partial v}{\partial z}) + \xi\frac{A_yuv}{xV_f} = -\frac{R}{\rho}\frac{\partial p}{\partial y} + G_y + f_y - b_y - \frac{R_{sor}}{\rho V_f}(v - v_w - \delta\cdot v_s) \quad (2)$$

$$\frac{\partial w}{\partial t} + \frac{1}{V_F}(uA_x\frac{\partial w}{\partial x} + vA_yR\frac{\partial w}{\partial y} + wA_z\frac{\partial w}{\partial z}) = -\frac{1}{\rho}\frac{\partial p}{\partial z} + G_z + f_z - b_z - \frac{R_{sor}}{\rho V_f}(w - w_w - \delta\cdot w_s). \quad (3)$$

Here, $(u, v, w)$ are the velocity components in coordinate directions $(x, y, z)$ respectively. For example, when Cartesian coordinates are used, $R = 1$ and $\xi = 0$, see FLOW3D manual [9]. $A_x$ is the fractional area open to flow in the $x$ direction, the same is also true for $A_y$ and $A_z$. Next, $V_F$ is the fractional volume open to flow, $R$ and $\xi$ are coefficients which depend on the coordinate system: $(x, y, z)$ or $(r, \theta, z)$, $\rho$ is the fluid density, $R_{sor}$ is a mass source term. Finally, $(G_x, G_y, G_z)$ are so called body accelerations [9], $(f_x, f_y, f_z)$ are viscous accelerations, $(b_x, b_y, b_z)$ are the flow losses in porous media or across porous baffle plates, and the final term accounts for the injection of mass at a source represented by a geometric component. Mathematical expressions for the viscous accelerations $(f_x, f_y, f_z)$ are presented in [10] and in the Appendix of [11]. Very useful information about FLOW3D and other fluid dynamics computer programs can be found in [12].

The term $U_w = (u_w, v_w, w_w)$ in equation (1) is the velocity of the source component, which will generally be non-zero for a mass source at a General Moving Object (GMO) [9]. The term $U_s = (u_s, v_s, w_s)$ is the velocity of the fluid at the surface of the source relative to the source itself. It is computed in each control volume as $\vec{U}_s = 1/\rho_s d(Q\vec{n})/dA$ where $dQ$ is the mass flow rate, $\rho_s$ fluid source density, $dA$ the area of the source surface in the cell and $\vec{n}$ the outward normal to the surface. The source is of the stagnation pressure type when in equations (1-3) $\delta = 0.0$ [9]. Next, $\delta = 1.0$ corresponds to the source of the static pressure type.

As we already mentioned, in all simulations we considered the blood flow as a pulsatile flow. The final result for the inflow waveform has been taken from figure 3 of work [13]. The pulse was applied for 5.5 cycle times in our work. These velocity values are used as time-dependent inflow initial boundary conditions. These numbers are included directly in the FLOW3D program.

Next, the general mass continuity equation, which is solved within the FLOW3D program has the following *general* form:

$$V_f\frac{\partial \rho}{\partial t} + \frac{\partial}{\partial x}(\rho u A_x) + R\frac{\partial}{\partial y}(\rho v A_y) + \frac{\partial}{\partial z}(\rho w A_z) + \xi\frac{\rho u A_x}{x} = R_{dif} + R_{sor}, \quad (4)$$

$R_{dif}$ is a turbulent diffusion term, and $R_{sor}$ is a mass source. The turbulent diffusion term is

$$R_{dif} = \frac{\partial}{\partial x}(v_p A_x\frac{\partial \rho}{\partial x}) + R\frac{\partial}{\partial y}(v_p A_y R\frac{\partial \rho}{\partial y}) + \frac{\partial}{\partial z}(v_p A_z\frac{\partial \rho}{\partial z}) + \xi\frac{\rho v_p A_x}{x}, \quad (5)$$

where the coefficient $v_p = C_p\mu/\rho$, $\mu$ is dynamic viscosity and $C_p$ is a constant. The $R_{sor}$ term is a density source term that can be used to model mass injections through porous obstacle surfaces.

### B. Turbulence and Viscosity Effects

Turbulence models can be taken into account in FLOW3D. This software allows us to estimate the influence of turbulent

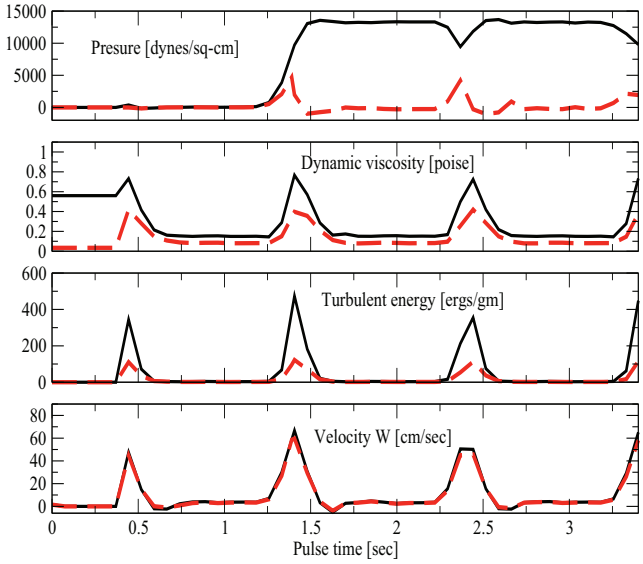


Fig. 1. Results for pressure, dynamic viscosity, turbulent energy and velocity W. Time-dependent results for the middle point of the cylinder. Bold black line calculations with non-Newtonian viscosity of the human blood; red dashed line with its Newtonian approximation.

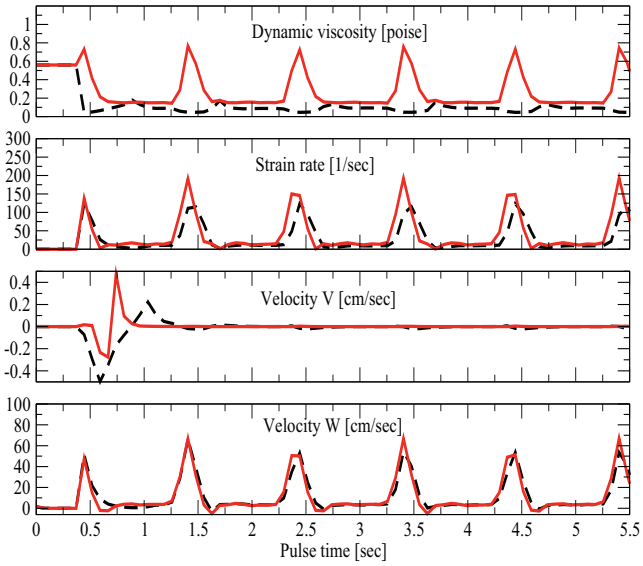


Fig. 2. Time-dependent results for a specific geometrical point inside the cylinder: the middle point. Black dashed line: simulations without taking into account the turbulence; red bold line results with the turbulence. The non-Newtonian viscosity is taken into account.

fluctuations on mean flow quantities. This influence is usually expressed by additional diffusion terms in the equations for mean mass, momentum, and energy. The turbulence kinetic energy per unit mass, $q$, is the following

$$\frac{\partial q}{\partial t} + \frac{1}{V_F}\left(uA_x\frac{\partial q}{\partial x} + vA_yR\frac{\partial q}{\partial y} + wA_z\frac{\partial q}{\partial z}\right) = P + G + Diff - D, \qquad (6)$$

where $P$ is shear production, $G$ is buoyancy production, $Diff$ is diffusion, and $D$ is a coefficient [9].

When the turbulence option is used, the viscosity is a sum of the molecular and turbulent values. For non-Newtonian fluids the viscosity can be a function of the strain rate and/or temperature. A general expression based on the Carreau model is used in FLOW-3D for the strain rate dependent viscosity:

$$\mu - \mu_\infty = \frac{\mu_0 E_T - \mu_\infty}{\lambda_{00} + \sqrt{[\lambda_0 + (\lambda_1 E_T)^2 e_{ij}e_{ij}]^{(1-n)}}} + \frac{\lambda_2}{\sqrt{[e_{ij}e_{ij}]}}, \qquad (7)$$

where $e_{ij} = 1/2(\partial u_i/\partial x_j + \partial u_j/\partial x_i)$ is the fluid strain rate in Cartesian tensor notations, $\mu_\infty, \mu_0, \lambda_0, \lambda_1, \lambda_2$ and $n$ are constants. Also, $E_T = exp[a(T^*/(T-b)-C)]$, where $T^*, a, b$, and $c$ are also parameters of temperature dependence, and $T$ is fluid temperature. This basic formula is used in our simulation of blood flow in vessels and in the aortic arch. For a variable dynamic viscosity $\mu$, the viscous accelerations have a special form.

The equations of fluid dynamics should be solved together with specific boundary conditions. The numerical model starts with a computational mesh, or grid. It consists of a number of interconnected elements, or 3D-cells. These 3D-cells subdivide the physical space into small volumes with several nodes associated with each such volume. The nodes are used to store values of the unknown parameters, such as pressure, strain rate, temperature, velocity components and etcetera. This procedure provides values used for defining the flow parameters at discrete locations and allows specific boundary conditions to be set up.

## III. SIMULATION RESULTS

Our simulation results are presented below. One of the most important preliminary testing tasks is to check for numerical convergence. This test has been successfully accomplished in this work. A portion of the test calculation results are shown bellow in this paper. Next, particular attention has been given to the calculation of wall shear stress distribution (WSS). WSS is the tangential drag force produced by moving blood. It is a mathematical function of the velocity gradient of blood near the endothelial surface:

$$\tau_w = \mu\left[\frac{\partial U(t,y,R_v)}{\partial y}\right]_{y\approx 0}. \qquad (8)$$

Here $\mu$ is the dynamic viscosity, $t$ is current time, $U(t,y,R_v)$ is the flow velocity parallel to the wall, $y$ is the distance to the wall of the vessel, and $R_v$ is its radius. It was shown, that the magnitude of WSS is directly proportional to blood flow/blood viscosity and inversely proportional to the cube of the radius of the vessel, in other words a small change in the radius of a vessel will have a large effect on WSS.

### A. Straight Vessel: Cylinder

First, we chose a simple vessel geometry, that is we considered the shape of a straight vessel to be a tube. In our simulations involving a straight cylinder type vessel we applied a cylindrical coordinate system: $(r, \theta, Z)$ with the axis $OZ$ directed over the tube axis. Different quantities of

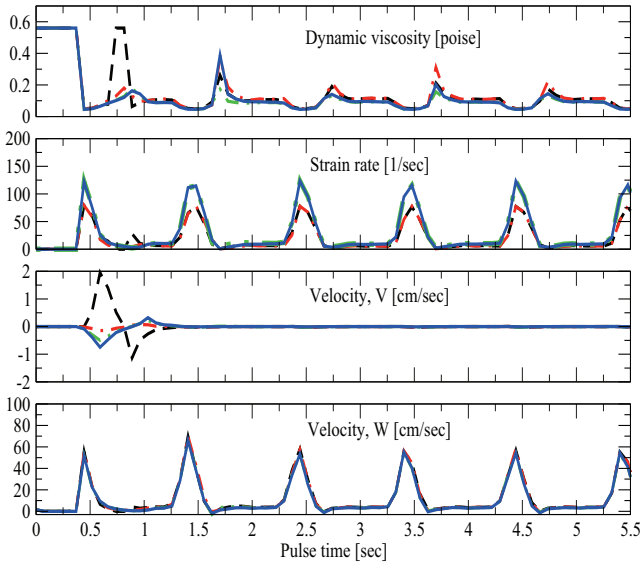


Fig. 3. Test of numerical convergence. Time-dependent dynamic viscosity, strain rate and velocity components V and W. Results for a vessel of simple geometry - cylinder type, for a specific spatial point inside the cylinder - the middle point. No turbulence effects are involved in these simulations with the realistic non-Newtonian viscosity of human blood. Black dashed line: calculations with 0.08 size for all cells [9], red dot-dashed line with 0.07, green double dot - dashed line with 0.065, and blue bold line calculations with 0.062 size for all cells.

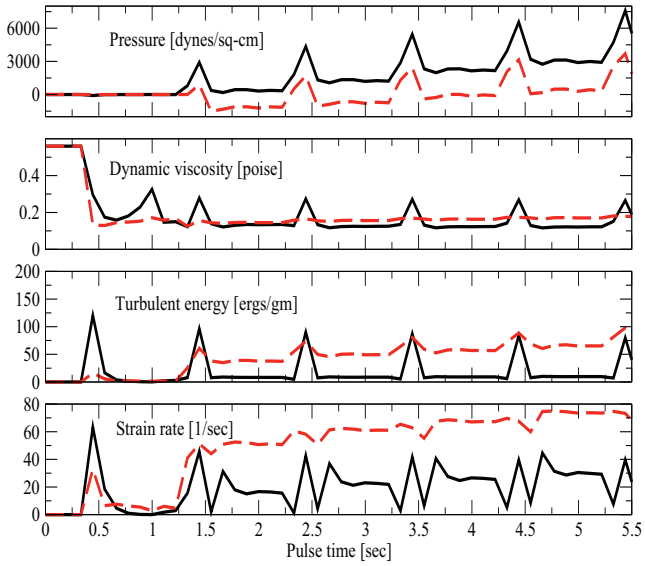


Fig. 4. Time-dependent results for a vessel with bifurcation. Pulsatile blood flow, non-Newtonian viscosity, and the turbulence effect is included. Bold black line: results for the far right outflow side $z = 0.0$; red dashed line results for the farthest up outflow side $y = 0.0$

cells have been used to discretize the empty space inside the tube. In the open space (inner part of the tube) the fluid dynamics equations have been solved using appropriate mathematical boundary conditions. The size of the tube is: $L = 8$ cm (in length) and $R = 0.34$ cm (length of inner radius). The thickness of the vessel wall is $s = 0.03$ cm. We have applied 5.5 cycles of blood pulse.

Time-dependent results for pressure, dynamic viscosity, turbulent energy and velocity component $W$ are presented in Fig. 1. It is very interesting to devise a comparison of the results using both a Newtonian and non-Newtonian viscosity. We apply the pulsatile flow and include turbulence, since it has proved to be important [11]. The turbulence effect is also shown in Fig. 2.

As one can see from Fig. 1, there are significant differences between these two calculations. Moreover, we specifically observed that when the two methods were applied our results for the pressure distribution, dynamic viscosity and turbulent energy disagree significantly. Thus, we arrive at the important conclusion: within a time-dependent (pulsatile) flow of human blood it is necessary to take into account turbulence and non-Newtonian viscosity.

Finally in this sections, time-dependent results for pressure, strain rate and velocity components $V$ and $W$ are presented in Fig. 3. The turbulent effects are not taken into account. We chose to present only one precise geometrical point for comparison purposes: the middle point: $r = \theta = 0$, and $Z = 4.0$ cm. The data for Fig. 3 were obtained with the non-Newtonian model of human blood. We refer the reader to the comments provided about the figure. We were able to closely replicate the values for all previous cell sizes [9] and obtain almost identical values. For example, pressure, wall shear stress and other parameters, for 0.065 and 0.062 cell sizes [9]. This means, that convergence has been achieved.

### B. Bifurcation and Aortic Arch

Below we show the result of our subsequent simulation involving a 90° bifurcated coronary artery, see Figs. 4 and 5. The geometrical model of the bifurcation consisted of a 90° intersection of two cylinders. This model represents the bifurcation between the left anterior descending coronary artery and the circumflex coronary artery.

In our opinion, in the case of pulsatile flow it is more interesting to present results in a time-dependent way. This method can provide a wider picture of highly non-stationary flow systems. In this paper, because of space limitations, we have just included time-dependent results for pressure, dynamic viscosity, turbulent energy, and strain rate. However, we understand, that results which depend on the spatial coordinates $(r, \theta, Z)$ for a few fixed moments of time are also highly useful.

In the case of the bifurcation shown in Figs. 4 and 5, we report the results for only two spatial points, which are the two outflow sides: the far right side and the farthest upper side of the bifurcation, see Fig. 5. The length of the lower horizontal vessel is 4 cm and its diameter is 0.54 cm. The length of the upper vertical vessel is 1.2 cm and its diameter is 0.4 cm. These sizes are consistent with average size human vessels.

Next, in Fig. 5 blood flows in from the left to the right with the imposed initial velocity profile taken from [10], [11], [13]. The pressure, strain rate and turbulent energy distributions are shown for only one specific time moment $t$=4.329 s. The velocity vectors are also shown on these plots. One can see, that the turbulence energy is higher in the region

of bifurcation. This effect should be taken into account in such computer simulations.

In Fig. 6 we present the results of strain rate distributions inside the arch for two specific time moments. At the far left point, which is the inlet, we specify the pulsatile velocity source as the initial condition. From the general theory of fluid mechanics it is then possible to determine using the blood density, viscosity, and spatial geometries, the dynamics of the blood according to the Navier-Stokes equation and its boundary conditions.

Blood flows from left to right in direction. However, because of pulsatility blood flows in the opposite direction too. The values obtained for the strain rate are also shown. These values strongly oscillate. From the plots one can conclude that in the region of the arch the strain rate values become much larger than in the region of the straight vessel. This result represents clear evidence that in this part of the human vascular system atherosclerotic plaques should localize less than in the straight vessels. However, the higher wall shear stress values in the aortic arch could be the reason for sudden mechanical disruption of the arterial wall in this part of the human vascular system. These computational results are consistent with laboratory and clinical observations [2].

## IV. CONCLUSION

In this work we applied computational fluid dynamics techniques to support pulsatile human blood flow simulations through different shape/size vessels and the aortic arch. The realistic blood pulse has been adopted and applied from work [13]. The geometrical size of the vessels and the aortic arch have been selected to match the average real values. Human blood was treated in two different ways: (a) as a Newtonian liquid when the viscosity of the blood has a constant value, and (b) as a non-Newtonian liquid with the viscosity value represented by the equation (7). The numerical coefficients in (7) have been taken from work [4].

It is always difficult to obtain a steady-state cycle profile and stable computational results at the very beginning of time-dependent simulations. However, after a short stabilization period a steady-state cycle profile can be obtained. In our simulations we used up to 5.5 pulse cycles to reach complete steady state profiles. We obtained valid results for pressure, wall shear stress distribution and other physical parameters, such as the three velocity components of blood flow. All of these were shown in Figs. 1, 2 and 3.

Our simulations showed that the FLOW3D program is capable of providing stable numerical results for all geometries included in this work. The time-dependent mathematical convergence test has been successfully carried out. Particular attention has been paid to this aspect of the calculations. It is a well known fact that fluid dynamics equations can have unstable solutions [3]. Therefore, numerical convergence has been tested and confirmed in this work.

The result of computer simulations of blood flow in vessels for three different geometries have been presented. For pressure, strain rate and velocity component distributions we found significant disagreements between our results obtained with the realistic non-Newtonian treatment of human blood and the widely used method in literature: a simple Newtonian approximation.

Our results are in good agreement with the conclusions of works [5], [14], where the authors also obtained significant differences between their results calculated with and without the non-Newtonian effect of blood viscosity. However, the recent work [15] should also be mentioned, in which the authors performed 2-dimensional simulations of human blood flow through the carotid artery with and without the non-Newtonian effect of the viscosity. They did not find any substantial differences in their results.

Next, the influence of a possible turbulent effect has also been investigated in this work. It was found that the effect is important. We believe, that the physical reason for this phenomena lies in the strong pulsatility of the flow and in the non-Newtonian viscosity of the blood. The contribution of the turbulence is most significant in the area of bifurcated vessels.

Finally, a significant increase of the strain rate and, the wall shear stress distribution, is found in the region of the aortic arch. This computational result provides additional evidence to support recent clinical and laboratory observations that this part of the human cardiovascular system is under higher risk of disruption [2], [16]. In future works it would be interesting to include the elasticity of the walls [17] of the aortic arch and other vessels.

## REFERENCES


[1] C.A. Taylor, M.T. Draney, Experimental and Computational Methods in Cardiovascular Fluid Mechanics, Annual Review of Fluid Mechanics 36, 197-231 (2004).

[2] Y.M. Carter, R.C. Karmy-Jones, D.C. Oxorn, G.S. Aldea, Traumatic Disruption of the Aortic Arch, European J. Cardio-thoracic Surgery, 20, 1231 (2001).

[3] L.D. Landau, E.M. Lifshitz, Fluid Mechanics, Volume 6, Pergamon Press Ltd., 1959.

[4] Y.I. Cho, K.R. Kensey, Effects of the non-Newtonian viscosity of blood on flows in a diseased arterial vessel. Part 1: Steady Flows, Biorheology 28, 241-262 (1991).

[5] J. Chen, X.-Y, Lu, J. of Biomechanics 37, 1899-1911 (2004).

[6] T. Rau, X. He, P. Venugopal, F. Vinuela, G. Duckwiler, and D. J. Valentino, Model. Simul. Engin., Vol. 2008, art. ID 691982.

[7] A.O. Frank, P.W. Walsh, and J.E. Moore Jr., Computational Fluid Dynamics and Stent Design, Artificial Organs 26(7), 614 (2002).

[8] I. Faik, R. Mongrain, R.L. Leask, J. Rodes-Cabau, E. Larose, O. Rertrand, Time-Dependent 3D Simulations of the Hemodynamics in a Stented Coronary Artery, Biomedical Materials 2, S28 (2007).

[9] FLOW-3D Users Manual, Version 9.2, Flow Science, Santa Fe, New Mexico, 2007.

[10] R.A. Sultanov, D. Guster, B. Engelbrekt, and R. Blankenbecler, in Proc. IEEE 11-th Intern. Conf. Comput. Sci. Engin., p.479, Sao Paulo, Brazil, 2008.

[11] R.A. Sultanov, D. Guster, arXiv:0811.1363v1 [physics:flu-dyn] 9 Nov 2008, Cornell University Library, online preprint service.

[12] T. Glatzel et al., Computers & Fluids, 37, 218 (2008).

[13] Y. Papaharilaou, J.A. Ekaterinaris, E. Manousaki, A.N. Katsamouris, J. Biomechanics 40, 367-377 (2007).

[14] J. Chen, X.-Y, Lu, Journal of Biomechanics 39, 818-832 (2006).

[15] J. Boyd, J.M. Buick, Phys. in Med. and Biol. 52, 6215 (2007).

[16] A. Pochettino, J.E. Bavaria, Aortic Dissection, in Book: Mastery of Cardiothoracic Surgery, Eds. L.R. Kaiser, I.L. Kron, T.L. Spray, Publisher: Lippincott Williams and Wilkins, September 2006.

[17] H. Fang, Z. Lin, Z. Wang, Lattice Boltzmann Simulation of Viscous Fluid Systems with Elastic Boundaries, Phys. Rev. E 57, R25-R28 (1998).

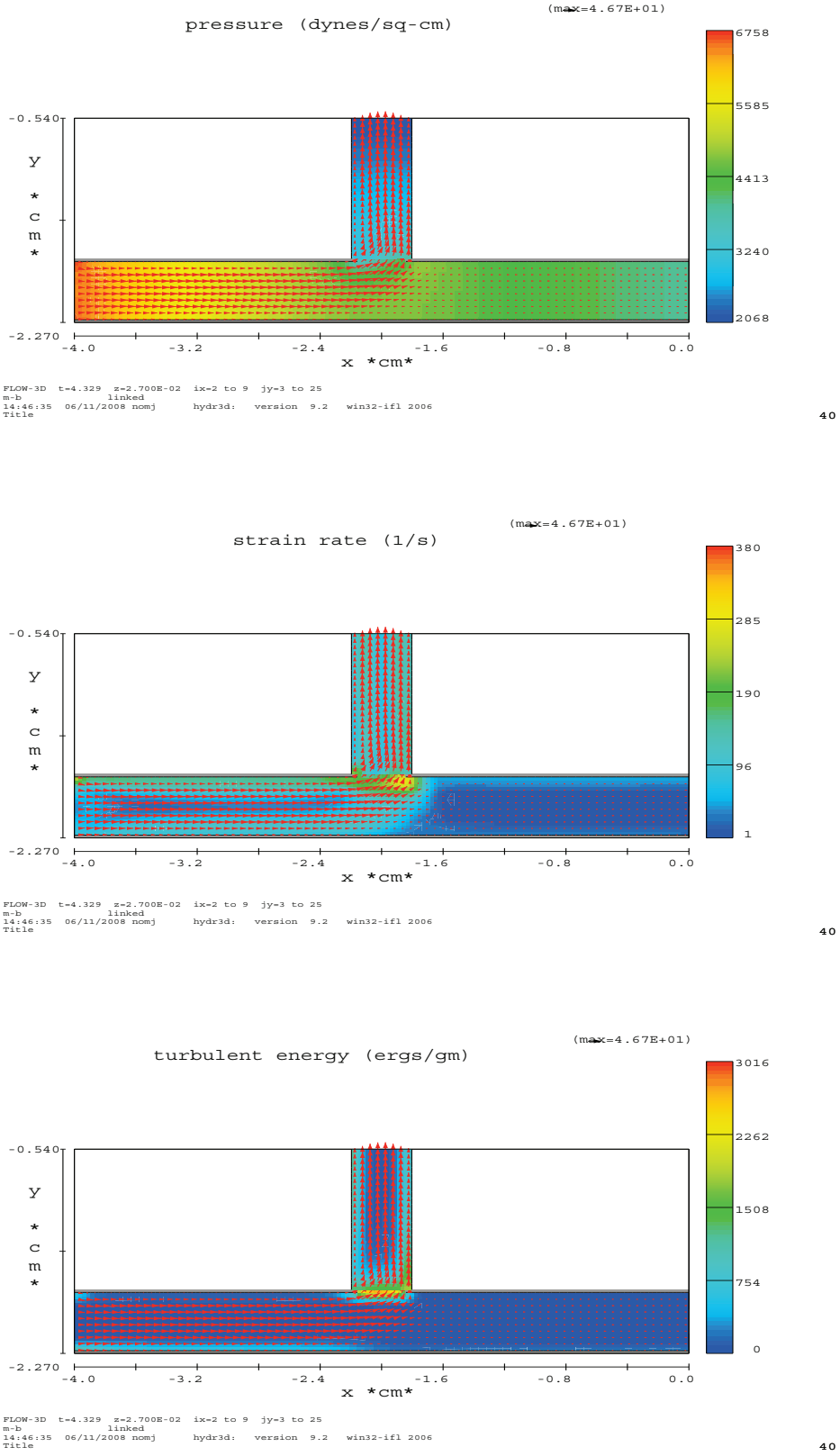


Fig. 5. The figures are 2D-plots showing the blood flow in the bifurcated vessels for only one precise moment of the discretized time $t_i = 4.329$ sec, the corresponding index is $i = 40$. The upper plot represents the result for the pressure distribution in the bifurcation, and the pressure ranges from 2068 dynes/sq-cm to 6758 dynes/sq-cm. The middle plot represents the results for the strain rate distribution and the lower plot shows results for the turbulent energy in the bifurcation. The range of the values is also shown.

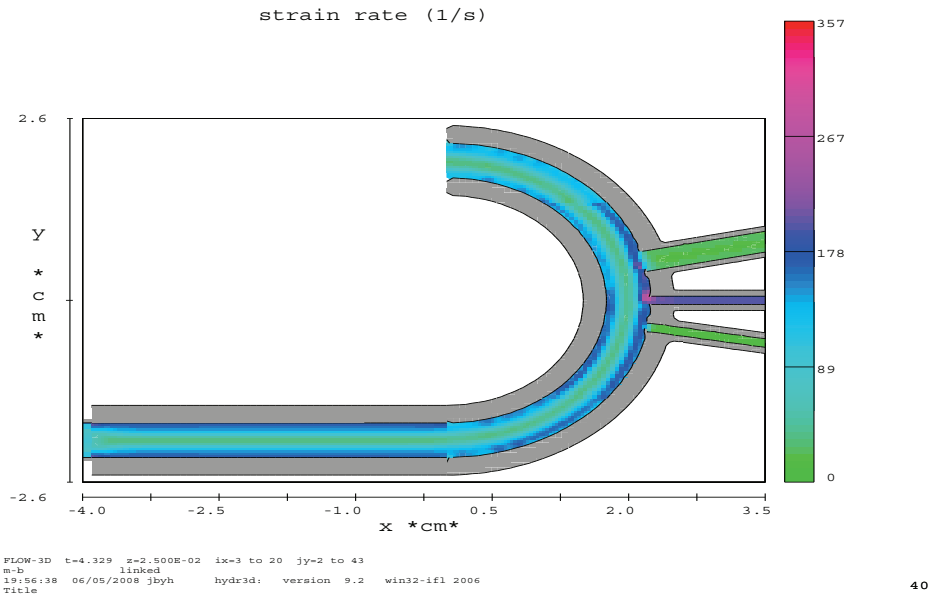


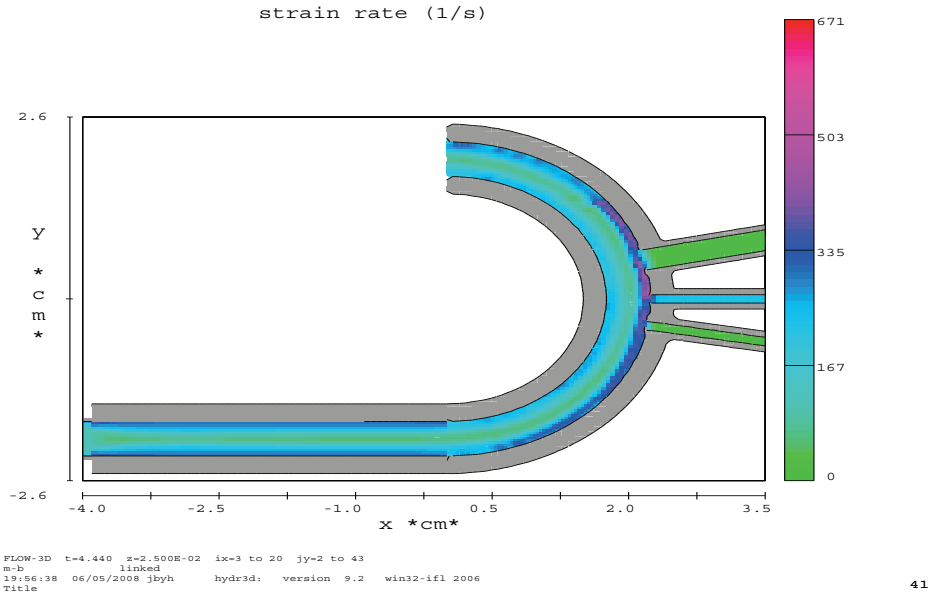


Fig. 6. Blood flow in the aortic arch. These two plots represent the full 2D-picture of the geometry used in these simulations. Shaded results for the strain rate are also shown, the bars on the right show the values. Results are for two specific moments of the times $t_{40}$ = 4.329 sec and $t_{41}$ = 4.440 sec. The values of the strain rate distribution range from 0.0 1/sec to 357.0 1/sec (upper plot) and from 0.0 to 671 1/sec (lower plot). The maximum values of the strain rate are localized in the region inside the arch.